Seasonal characterization of CDOM for lakes in semi-arid regions of Northeast China using excitation-emission matrices fluorescence and parallel factor analysis (EEM-PARAFAC)

Ying Zhao[1], Kaishan Song[1*], Zhidan Wen[1], Lin Li[2], Shuying Zang[3], Tiantian Shao[1], Sijia Li[1], Jia Du[1]

[1]Northeast Institute of Geography and Agroecology, Chinese Academy of Sciences, Changchun, Jilin, 130102, China

[2]Department of Earth Sciences, Indiana University-Purdue University, Indianapolis, IN, USA

[3]College of Geographical Science, Harbin Normal University, Harbin, China

*corresponding author E-mail: songks@iga.ac.cn; Tel: 86-0431-85542364

Abstract. The seasonal characteristics of fluorescent components in CDOM for lakes in the semi-arid region of Northeast China were examined by excitation-emission matrix (EEM) spectra and parallel factor analysis (PARAFAC). Two humic-like (C1 and C2) and the protein-like (C3 and C4) components were identified using PARAFAC. The average fluorescence intensity of the four components differed under seasonal variation from June and August 2013 to February and April 2014. Components 1 and 2 exhibited strong linear correlation (R^2 = 0.633). Significantly positive linear relationships between CDOM absorption coefficients a(254) (R^2 = 0.72, 0.46, $p < 0.01$), a(280) (R^2 = 0.77, 0.47, $p < 0.01$), a(350) (R^2 = 0.76, 0.78, $p < 0.01$) and F_{max} for two humic-like components (C1 and C2) were exhibited, respectively. A

significant relationship (R^2 = 0.931) was found between salinity and DOC. However, almost no obvious correlation was found between salinity and EEM-PARAFAC extracted components except for C3 (R^2 = 0.469). Results from this investigation demonstrate that the EEM-PARAFAC technique can be used to evaluate the seasonal dynamics of CDOM fluorescent components for inland waters in the semi-arid regions of Northeast China, and to quantify CDOM components for other waters with similar environmental conditions.

Keywords: CDOM, fluorescent components, EEMs, PARAFAC, DOC, Salinity

1 Introduction

Dissolved organic matter (DOM), a heterogeneous mixture of humic acids, proteins and carbohydrates, plays important roles in aquatic ecosystems (Zhang et al., 2010). Chromophoric dissolved organic matter (CDOM), the colored fraction of DOM, absorbs light energy in the ultraviolet (UV) and visible region of the spectrum and inhibits the propagation of UV radiation. CDOM in waters also affects the transport and bio-availability of materials such as trace metals and other pollutants (Song et al., 2013), so it can be used as a proxy of water quality. In natural water bodies, CDOM originates from the degradation of plant materials and other organisms and terrestrially imported substances, which varies in time and space and is controlled by its structure and composition (Stedmon et al., 2003). CDOM is compositionally complex, making it difficult for us to isolate hydrophobic from hydrophilic acids using XAD ion-exchange resins (Aiken et al., 1992; Spencer et al., 2010).

Nonetheless, some optically active components of CDOM can emit fluorescence after absorbing light at certain wavelengths (Zhang et al., 2010) so that the fluorescence spectroscopic techniques can be used to provide detailed information about the source and concentration of CDOM. The traditional fluorescence techniques including fluorescence emission spectrometry and synchronous fluorescence scanning applied to examine CDOM components have the drawback that the output was restricted to a linear scan (Hudson et al., 2007).

Recently, excitation-emission matrix fluorescence spectroscopy (EEM) has been applied to identify CDOM components because of this ability of producing synchronous scan spectra in the form of contours (Stedmon et al., 2003; Zhang et al., 2010). The EEM spectroscopy is considered the most effective technique for studying the composition of fluorophores given its high selectivity and sensitivity to CDOM in water columns (Zhang et al., 2010). In recent years, EEM spectroscopy has been widely used to distinguish allochthonous and autochthonous CDOM source in aquatic environment (Coble et al., 1998; Mayer et al., 1999; Yamashita et al., 2008, 2010; Zhang et al., 2013), and to investigate the dynamics of marine, freshwaters and ice-water ecosystems as well as snow melting water (Barker et al., 2006, 2009, 2010, 2013; Coble, 2007; Fellmanet al., 2010; Guo et al., 2010; Hudson et al., 2007; Stedmon et al., 2007). Based on the peak positions in EEMs, two main fluorescent components, i.e., humic-like and protein-like substances, have been identified and investigated (DelCastillo et al., 1999; Jaffe´ et al., 2004). However, overlapped fluorophores of CDOM EEMs could make this traditional ‘peak-picking’ method

unreliable to evaluate CDOM dynamics in aquatic ecosystems (Coble, 1996; Stedmon et al., 2003). Recently, the combined EEMs-PARAFAC (parallel factor analysis) technique has been shown to effectively decompose EEM of CDOM into independent fluorescent components and assess the source of CDOM and relationships with other water quality parameters (Broisover et al., 2009; Guo et al., 2010; Zhang et al., 2010, 2011, 2013). Stedmon et al. (2003) introduced PARAFAC and identified five distinct DOM components for a Danish estuary and its catchment (Stedmon et al., 2003). In coastal environments, Yamashita et al. (2008) reported on seven components using the combined EEMs-PARAFAC technique and assess the dynamic of individual fluorophores and relationship with salinity in Ise Bay. Zhang et al. (2011) also found three different components by PARAFAC modeling and analyzed the correlations between the fluorescent components and absorption coefficients of CDOM for Lake Tianmu and its catchment.

The Songnen Plain is a fluvial plain with semi-arid climate, in which many fresh and brackish waters are distributed due to its geomorphology (Song et al., 2013). Dissolved organic carbon (DOC) characterisitics of these fresh and brackish waters across the Songnen Plain have been studied by Song et al. (2013); the results indicated that a huge amout of DOC were stored in these waters. In particular, brackish waters would exhibit high average DOC concentration and significantly contributed the carbon budget to inland waters (Duarte et al., 2008; Song et al., 2013; Tranvik et al., 2009). However, little studied has been made on the detailed information of DOC sources for these waters in the Songnen Plain. Therefore, it

90 motivated us to investigate the components in CDOM for both fresh and brackish
91 waters in the semi-arid region. In the present study, the absorption and fluorescence of
92 CDOM were determined for the water samples collected from seven lakes in the
93 western part of Jilin province, which had seasonal variation. The specific objectives of
94 this study are to: 1) characterize CDOM components contained in these lakes using
95 EEMs and their origins through the EEM-PARAFAC method; 2) assess the dynamic
96 of individual fluorescent component of CDOM under seasonal variation; and most
97 importantly 3) link CDOM fluorescence intensities, absorption coefficients, DOC
98 concentrations and salinity to each other.
99

100 # 2 Materials and Methods

101 ## 2.1 Lakes and water sampling

102 The water bodies investigated in this study were located in the western part of Jilin
103 Province, which belongs to the semi-arid part of the Songnen Plain (Song et al., 2013).
104 Two groups of lakes were investigated, i.e., the Chagan lake group and the Yuelianghu
105 lake group. The Chagan lake group is made up of Lake Chagan (CGL), Xinmiaopao
106 (XMP), Xindianpao (XDP) and Kulipao (KLP). The Yuelianghu lake group mainly
107 includes Lake Yueliang (YLL), Talahong (TLH) and Xinhuangpao (XHP) (Fig. 1).
108 The primary economic value for these lakes is fishery, agricultural irrigation and
109 recreation. The average annual precipitation is about 391 mm, but the average
110 evaporation is up to 1790 mm, resulting in water scarcity. Due to the area dominated
111 by saline-alkali soil, the rainfall flush and agricultural catchment land use can result in

an increase of lake salinities. In order to characterize the CDOM fluorescent components under seasonal variation using EEMs-PARAFAC, 67 water samples were collected from the surface of the seven lakes in 1-liter acid-cleaned plastic bottles during four field campaigns in June and August 2013 as well as in February and April 2014, respectively. These samples were collected during the ice covering period using an ice drilling auger. After the ice layer was drilled a hole, the under-ice surface water was coming up. The ice shavings were collected in plastic bags and the under-ice surface water was collected in plastic bottles. The collected samples were held on ice and immediately transported to the laboratory in the Changchun City of Jilin province within 3-5 hours. In the laboratory, these samples were kept at 4 ℃ until analysis after filtered within two days. Latitude and longitude of each sample location were recorded *in situ* using a Trimble Global Positioning System (GPS).

Figure 1. Locations of the water sampling sites for 7 lakes in the western part of Jilin province, Northeast China.

2.2 Analytical procedures

To characterize the basic parameters of water quality, salinity was measured through a DDS-307 electrical conductivity (EC) meter in laboratory. Salinity was expressed in the basis of the UNESCO practical salinity unit (PSU 1978). The pH was measured using a PHS-3C pH meter at room temperature (20 ± 2 ℃) in laboratory. Water turbidity was determined using the Shimadzu UV-2600PC UV-Vis dual beam spectrophotometer with matching 3 cm quartz cells at room temperature (20 ± 2 ℃)

135 with Milli-Q water as the reference. To determine DOC concentrations, water samples
136 were filtered through 0.45 μm filters and then measured using a Shimadzu TOC-5000
137 Analyzer and a 1.2 % Pt on silica catalyst at 680 ℃. Potassium hydrogen phthalate
138 was used as standard. The reproducibility of the analytical procedure was within 2-3 %
139 for the current study (APHA, 1998; Song et al., 2011).
140

141 **2.3 Absorption measurement**

142 In laboratory, all the samples were filtered at low pressure, first through a
143 pre-combusted Whatman GF/F filter (0.7 μm), and then through a pre-rinsed 25 mm
144 Millipore membrane cellulose filter (0.22 μm) into glass bottles. Absorption spectra of
145 the samples were measured between 200 and 800 nm at 1 nm increments using the
146 Shimadzu UV-2600PC UV-Vis dual beam spectrophotometer with a 1 cm quartz
147 cuvette and Milli-Q water as reference. The absorption coefficient a_{CDOM} was
148 calculated from the measured optical density (OD) of the sample using Eq. (1):

149 $$a_{CDOM}(\lambda) = 2.303[OD_{S(\lambda)} - OD_{(null)}]/\gamma \quad (1)$$

150 where γ is the cuvette path length (0.01 m) and the factor 2.303 converts from base 10
151 to base natural logarithm transformation. Some fine particles possibly remained in the
152 filtered solution (Babin et al., 2003; Bricaud et al., 1995), therefore it is necessary to
153 correct for scattering by fine particles and in this case, $OD_{(null)}$ is the average optical
154 density over 740-750 nm where the absorbance of CDOM can be assumed to be zero.

155 A CDOM absorption spectrum ($a_{CDOM}(\lambda)$) can be expressed as an exponential
156 function (Babin et al., 2003; Bricaud et al., 1995):

$$a_{CDOM}(\lambda_i) = a_{CDOM}(\lambda_r)\exp[-S(\lambda_i - \lambda_r)] \quad (2)$$

where $a_{CDOM}(\lambda_i)$ is the CDOM absorption at a given wavelength λ_i, $a_{CDOM}(\lambda_r)$ is the absorption estimate at the reference wavelength λ_r(440 nm), and S is the spectral slope of the CDOM absorption. According to Helms et al. (2008), S is calculated by fitting a linear model to the date over a wavelength range of 275 to 295 nm (*S1*) or 350 to 400 nm (*S2*). To eliminate the inter-laboratory variability, the slope ratio S_R= *S1*/*S2* is defined to indicate the molecular weight and photo-bleaching of CDOM (Helms et al., 2008; Zhang et al., 2010).

2.4 Three-dimensional fluorescence measurement

The EEMs analysis of CDOM were conducted using a Hitachi F-7000 fluorescence spectrometer (Hitachi High-Technologies, Tokyo, Japan) with a 700-voltage xenon lamp. The scanning ranges were 200–450 nm for excitation, and 250–500 nm for emission. Readings were collected in the ratio mode at 5 nm intervals for excitation, and at 1 nm intervals for emission, using a scanning speed of 2400 nm min^{-1}. The band-passes were 5 nm for both excitation and emission. A Milli-Q water blank of the EEMs was subtracted to eliminate the water Raman scatter peaks (McKnight et al., 2001; Stemdon et al., 2003; Zhang et al., 2010, 2011).

The inner-filter effect, which results from reabsorption and excitation of the fluorescence itself, can reduce the fluorescence intensity by 5% (Larsson et al., 2007; McKnight et al., 2001). In order to eliminate the inner-filter effect, the EEMs were corrected for absorbance by multiplying each value in the EEMs with a correction

factor based on the assumption that the average path length of absorption of the excitation and emission light is one-half length of the cuvette (McKnight et al., 2001; Zhang et al., 2010). The correction function is expressed as follows:

$$F_{corr} = F_{obs} \times 10^{(A_{ex}+A_{em})/2} \quad (3)$$

where F_{Corr} and F_{obs} are the corrected and uncorrected fluorescence intensities and A_{ex} and A_{em} are the absorbance values at the respective excitation and emission wavelengths.

Finally, the fluorescence intensities of all sample's EEMs were normalized to the area under the Milli-Q water Raman peak (λex=350 nm, λem=371-428 nm) measured daily (Lawaetz and Stedmon, 2009). The contour figures of the EEMs were plotted using the Matlab 10.0 software package (Math Works, Natick Massachusetts, America).

2.5 The PARAFAC modeling

PARAFAC, a three-way method, is applied to decompose the CDOM fluorescence into separate fluorescent signals (Andersen and Bro, 2003; Stedmon and Bro, 2008). A number of investigators have used EEMs-PARAFAC to characterize DOM in freshwater and marine aquatic environments (Cory et al., 2005; Stedmon and Markager, 2005; Yamashita, 2008; Zhang et al., 2010, 2011). According to Stedmon and Bro (2008), a similar PARAFAC analysis is carried out in the present study using the DOMFluor toolbox in MATLAB with the "N-way toolbox for MATLAB"

(Andersson et al., 2000). Before PARAFAC modeling, the excitation wavelengths from 200 to 220 nm and the emission wavelengths from 250 to 300 nm were deleted because of their poor quality. In order to remove the effect of Rayleigh scatter on PARAFAC modeling, the missing values (NaN-Not a number) were inserted in the regions ($Ex\text{-}20 \leqq Em \leqq Ex+20$ and $2Ex\text{-}20 \leqq Em \leqq 2Ex+20$; unit: nm) which are significantly influenced by the first and second order scattering from the measured spectroscopic data (Hua et al., 2007; Stedmon and Bro, 2008).

To determine the appropriate number of PARAFAC components, the split-half validation procedure was executed to verify whether the model was valid by comparing the emission and excitation loadings from each half (Stedmon and Bro, 2008). Split-half analysis is the most effective method for implementing the PARAFAC models, in which the EEMs are randomly divided into four groups of equal size, and then analyzed for two half splits (1-2 and 3-4 half) respectively. If the correct number of components is chosen, the excitation and emission loadings from the two groups should show the same shape and size (Bro, 1997, 1999). The fluorescence intensity of every component was represented by F_{max} (Raman unit: nm^{-1}) (Stedmon and Markager, 2005).

2.6 Statistical analysis

Statistical analysis was conducted using the SPSS 16.0 software package (Statistical Program for Social Sciences). Regression and correlation analysis was used to describe the relationship between CDOM absorption coefficient, DOC concentration,

223 salinity and F_{max}. The difference is considered to be statistically significant when
224 *p*-values are less or equal to 0.05.
225
226 # 3 Results and discussion
227 ## 3.1 Water quality conditions
228 The water quality parameters, i.e., pH, salinity, turbidity for the 67 water samples
229 collected from June 2013 to April 2014 in the western part of Jilin province are
230 displayed in Table 1. When the set of samples from various field trips was pooled
231 together, the waters had high pH values (mean, 8.55) and high salt contents (mean,
232 0.48 PSU). The highest salinity (0.70 PSU) was present when the lakes were frozen in
233 February 2014, whereas relatively constant values (around 0.40 PSU) were exhibited
234 in other three seasons. Also the water bodies were highly turbid with the mean of
235 62.18 ± 79.07 NTU. The highest turbidity was present in June 2013, and then reduced
236 in August 2013, and the lowest value was recorded in February 2014. Compared with
237 February 2014, the turbidity had almost no change in April 2014 (Table 1).
238
239 **Table 1. Mean value of water quality parameters from June 2013 to April 2014.**
240
241 ## 3.2 EEMs characterization of CDOM
242 Based on the EEMs 'peak picking' technique, the key fluorescence peaks can be
243 observed in 67 water samples: two humic-like and two protein-like substances (Coble,
244 1996; Stedmon et al., 2003). The humic-like components are the mixture of aromatic

and aliphatic compounds-humic-like acids from terrestrial substances, and aquatic humic-like substances of phytoplankton origin. With respect to the protein-like components, i.e., tyrosine-like and tryptophan-like substance, mainly consist of dissolved amino acids. As an example, Fig. 2 displays the EEMs of samples from lake Xindianpao at different seasons. The peaks comprise two humic-like fluorescence peaks: one in the ultraviolet range (Ex/Em = 220-240/410-430 nm) and the other in the visible range (Ex/Em = 300-340/410-450 nm) and the protein-like fluorescence peaks: tyrosine-like (Ex/Em = 210-230, 270-280/310-330 nm) and tryptophan-like (Ex/Em = 220-230, 280-300/350-370 nm). The measured fluorescence intensity is dependent on the concentration of the dissolved fluorophores in water bodies. The fluorescence properties of CDOM had seasonal variation. For Xindianpao, the protein-like fluorescence peaks were higher than the humic-like fluorescence peaks in June 2013, whereas the humic-like fluorescence peaks were higher than the protein-like peaks in August 2013.

Figure 2. Examples of EEMs for one water sample from Xindianpao Lake in the western part of Jilin province at different seasons a) June 2013; b) August 2013; c) February 2014; d) April 2014 (Fluorescence is in Raman unit: nm^{-1}).

In split-half analysis, the 67 EEMs were randomly divided into four halves and then analyzed for two different splits (1-2 and 3-4 half split). When the number of components was chosen to be four, the excitation and emission loadings from the output results of the 1-2 and 3-4 split-half analysis largely overlapped, respectively

(Fig. 3). It should be noted that for the 3-4 split-half analysis, the excitation and emission loadings of component 3 and component 4 were reversed. In fact, the output results of the split-half analysis were valid as long as the excitation and emission loadings of the fluorescent component were overlapped at the same wavelength and these components in different colors in the two groups only represent the order of appearance of the components according to their contributions (Stedmon and Bro, 2008).

Figure 3. Results from split-half analysis (1-2 top a); 3-4 down b)) in PARAFAC models. The plots represent spectral shapes of the excitation and emission loadings from the two halves (1-2; 3-4 split -half analysis) modeling.

In our study, four separate fluorescent components (Fig. 4a-d) and the excitation and emission loadings (e-h) of the four components identified by EEM-PARAFAC are summarized in Fig. 4 and Table 2. The first fluorescent component (C1) was a biological degradation humic-like component that displays two excitation maxima (at 230 and 300 nm) with a single emission wavelength (at 425 nm) comparable to humic-like peaks (M and N) in marine and in phytoplankton degradation experiments for inland waters (Coble, 1996; Zhang et al., 2009). Component 2 had the maximum excitations (at 255 and 350 nm) and an emission wavelength (at 460 nm) (Fig. 4a-b), which was consistent with the humic-like peaks (A and C) defined by Coble (1996). Component 3 demonstrated two excitation maxima (at 225 and 275 nm) and one emission maximum (at 360 nm), which

resembles the tryptophan-like (T) component as found by Baker et al. (2004) and Hudson et al. (2007). For component 4, it is likely related to tyrosine-like component (B), which was characterized by the maximum excitations at 225 and 275 nm and the emission wavelength was found at 310 nm. Components 3 and 4 represent autochthonous semi-labile CDOM associated with bacteria activity and phytoplankton degradation (Borisover et al., 2009; Stedmon et al., 2003). Particularly, there was a shoulder at the excitation wavelength 310-330 nm in component 3 and 330-340 nm in component 4, which may be due to the residual Raman peaks in some water samples (Fig. 4c-d). In this study, not all of the four components were present in all of the samples.

Figure 4. The PARAFAC modeling output shows the contour plots of the four PARAFAC fluorescent components (a-d) and excitation (black) and emission (red) loadings (e-h) of each component. Fluorescence is in Raman units: nm^{-1}.

Table 2. Positions of the fluorescence maximum peaks of the four components identified by PARAFAC modeling in the present study compared with those previously identified. Secondary excitation maxima is given in brackets.

3.3 Temporal distribution of PARAFAC components

As shown in Fig. 5a and b, the average fluorescence intensity of the four components had seasonal variation. When all the water samples at different seasons were pooled together, the average value of total fluorescence intensity was 2.05 ± 0.93 nm^{-1}, corresponding to the intensities of 0.71 ± 0.32 (C1), 0.33 ± 0.11 (C2), 0.50 ± 0.24

315 (C3), and 0.51 ± 0.26 (C4) nm^{-1} for different components. These results can
316 demonstrate that the fluorescence intensity was dominated by C1, implying most part
317 of the CDOM for the seven inland lakes was originated from phytoplankton
318 degradation and other organisms. The protein-like components (C3 and C4), related to
319 bioavailability and microbial activity of CDOM, had almost the same magnitude. At
320 all four seasons, the fluorescent component C2, which was terrestrially imported to
321 water bodies, contributed less to total fluorescence than the other three. The total
322 fluorescence intensity differed under seasonal variation, varying from 2.54 ± 0.68
323 nm^{-1} in June to 1.93 ± 0.70 nm^{-1} in August 2013, and then increased to 2.34 ± 0.92
324 nm^{-1} in February and reduced to the lowest 1.57 ± 0.55 nm^{-1} in April 2014 (Fig. 5b).
325 The intensities of four fluorescent components (i.e., 0.75 ± 0.17 (C1), 0.32 ± 0.06
326 (C2), 0.69 ± 0.24 (C3), and 0.77 ± 0.20 (C4) nm^{-1}) from the samples collected in June
327 2013 exhibited similar trends to that for the pooled data set. These values were higher
328 than the seasonal average except C2 (0.32 ± 0.06 nm^{-1}). This can be explained by
329 enhanced activities from plant degradation and microbial activities, but less terrestrial
330 substances were imported to the water bodies in June and therefore the fluorescence
331 intensity of C2 was lower than the seasonal average. Compared to the fluorescence
332 intensity in June, the three fluorescence intensities (0.65 ± 0.14 (C1), 0.33 ± 0.16 (C3),
333 0.52 ± 0.36 (C4) nm^{-1}) from the samples collected in August 2013 reduced, but an
334 increased value was recorded for C2 (0.42 ± 0.05 nm^{-1}). Especially, the fluorescence
335 intensities of two protein-like components showed an obvious difference. This can be
336 attributed to substantially increased precipitation up to 180 mm in July from June to

337 August 2013 (Fig. 5c) so that flood occurred when rainfall continued to increase in
338 August. Gradually, DOM contained in terrestrial CDOM was flushed by rainfall to the
339 lakes so that the C2 (0.42 ± 0.05 nm^{-1}) fluorescence intensity became higher. In
340 accordance with Cheng et al. 2010, the rainwater CDOM for this study was largely
341 characterized by protein-like components (Cheng et al., 2010). The fluorescence
342 intensity of the rainwater CDOM was very weak, and also the rainwater CDOM
343 contained much lower humic-like concentration (Fig. 6b). The intensities of the other
344 three components decreased because of dilution resulting from heavy rain and
345 relatively weak microbial decomposition of plants.

346 The highest C1 (1.02 ± 0.38 nm^{-1}) presented in February 2014 and the C2 (0.39
347 ± 0.12 nm^{-1}) intensity remained almost the same as that in August 2013. However, the
348 protein-like components indicated that the C3 (0.57 ± 0.25 nm^{-1}) intensity was higher
349 than the C4 (0.35 ± 0.17 nm^{-1}) intensity, which was opposite to the results from other
350 months (Fig. 5b). In cold winter, the surface waters formed a thick layer of ice
351 covering the lake waters. Because the ice cover reduced light penetration and
352 restricted gas exchange between the underlying water and atmosphere, vigorous
353 biological activities in the lakes would be prohibited at low temperature and low light
354 level (Thomas K., 1983; Uusikiv et al., 2010; Wharton, et al., 1993). Also, dissolved
355 matters were left in the underlying surface waters and little terrestrial matters were
356 imported to the lakes once covered by ice (Stedmon et al., 2007). Therefore, the C1
357 and C3 in the water of the lakes beneath the ice layers would cumulate simultaneously,
358 whereas, the C2 remained the same. Obviously, the fluorescence intensity of

component 1 reached the highest value for the winter samples. As shown in Fig. 6a, another striking feature for the winter samples was that the fluorescence of CDOM in the ice was dominated by the tyrosine-like C4 component, which is consistent with the findings of Barker et al. (2009, 2013) and Stedmon et al. (2007). It showed that the C4 component was left in the ice-cover when the lakes were frozen. Therefore, it is not surprising that the intensity of component C4 for water beneath ice layers was reduced and the concentrated C3 showed a much higher fluorescence intensity. In April 2014, the intensities of four fluorescent components (0.47 ± 0.17 (C1), 0.25 ± 0.08 (C2), 0.40 ± 0.16 (C3), and 0.45 ± 0.13 (C4) nm^{-1}) exhibited similar seasonal trends though these values were much lower than the average. Our interpretation is that the ice CDOM was characterized by tyrosine-like component (C4) (Fig. 6a), and the fluorescence intensity of C4 contributed by the ice-melt water was very weak. However, the underlying lake CDOM was dominated by both humic-like (C1 and C2) and protein-like (C3 and C4) components. When the ice in the lakes melt into water with warming weather and biological degradation and human activity was weak, the lake CDOM was diluted by the ice-melted water and the fluorescence intensity would reach to the lowest value in early spring.

Figure 5. a) Seasonal average of F_{max} for EEM-PARAFAC components (C1, C2, C3 and C4) for lakes in the western part of Jilin province; b) Seasonal variation of the four EEM-PARAFAC components at different seasons; c) Monthly variation of rainfall for the lakes in western part of Jilin province from April 2013 to February 2014. The error bar represents standard deviations.

383 **Figure 6. Representative examples of EEMs for a) lake ice-melt water sample, and b)**
384 **rainwater CDOM in the western part of Jilin province (Raman: nm^{-1}).**
385
386 ### 3.4 CDOM versus EEM-PARAFAC extracted components
387 The concentration of DOC, CDOM absorption coefficients and the slope ratio S_R are
388 shown in Table 3. The DOC concentrations ranged from 10.03 to 88.15 mg L^{-1} during
389 the study period, with an average value of 37.60 ± 18.05 mg L^{-1}. It is because the
390 prolonged sunshine duration can result in an evapo-condensed DOC concentration in
391 the Songnen Plain. The highest averaged DOC concentration (55.04 ± 20.00 mg L^{-1})
392 was present in February 2014; whereas, relatively constant values of approximate 30
393 mg L^{-1} were observed in the other three seasons, demonstrating a seasonal dynamics
394 that can be attributed to hydrological, climatic and landscape variations (Song et al.,
395 2013). This can be attributed to the accumulated DOC when the lakes freeze in winter,
396 which leaves DOC in the liquid phase, resulting in a higher DOC concentration in the
397 underlying water (unpublished material). Generally, the absorption coefficient a(350)
398 was used as a proxy for characterizing CDOM concentration, which was 5.73 ± 1.68
399 m^{-1} in June 2013, 5.82 ± 0.81 m^{-1} in August 2013, 6.36 ± 2.17 m^{-1} in February 2014,
400 4.17 ± 1.49 m^{-1} in April 2014, respectively, with an seasonal average of 5.40 ± 1.84
401 m^{-1}. The highest averaged CDOM absorption coefficients a(350), a(280), a(254) were
402 also present in February 2014, corresponding to the highest DOC concentration. The
403 S_R values of the two wavelength ranges (275-295 nm over 350-400 nm) were used to
404 represent the ratio of molecular weight of humic acid and fulvic acid. The mean of S_R
405 for all water samples was up to 1.21 ± 0.20, with the lowest 0.96 ± 0.22 in August

2013 suggesting the relatively weak microbial decomposition of plants and lots of terrestrially imported substances through rainwash resulted in the higher average molecular weight of DOC.

Table 3. Mean values of DOC concentration and CDOM absorption coefficients groups at different seasons. S_R: the slope ratio of $S_{275\text{-}295nm}$: $S_{350\text{-}400nm}$.

When the whole data set (N = 67) was pooled together, there were significantly positive linear relationships between a(254), a(280), a(350) and F_{max} for two humic-like components (C1 and C2), respectively, but mostly such correlations were not observed for the protein-like components (Fig. 7, Table 3). These results were in accordance with previous investigations (Zhang et al., 2010, 2011). Components 1 and 2 were strongly linearly correlated with each other (R^2 = 0.633), indicating that the concentrations of the two humic-like components were controlled by common sources. There was a weak relationship (R^2 = 0.051) between the protein-like components (C3 and C4) because of a complex origin of CDOM such as rainfall in summer, ice in winter and organic pollutants derived from domestic, agricultural and industrial sewerage, which represent the complex origins of CDOM. However, there was almost no correlation between the humic-like and protein-like components. The linkage of a fluorescence signal to DOC was very complicated because of the seasonal effects of both steady and labile fluorescence and non-fluorescence CDOM components as a result of increased rainfall and algal blooms which affect the DOC concentration (Henderson et al., 2009). Component 3 of the CDOM fluorescence can

be used to detect water pollution (Baker et al., 2004). A weak relationship ($R^2 = 0.42$) (Fig. 7d) was found between DOC and component 3 from the decay of plants through microbial activity or the pollution from human and animal wastes.

The most important finding for the water samples collected at different seasons from the Songnen Plain is a significant relationship ($R^2 = 0.931$) between salinity and DOC (Fig. 7e), which implies that a prolonged sunshine duration can result in an evapo-condensed DOC concentration. Different from the findings by Yamashita et al. (2008) for ocean water, this study did not find obvious correlation between salinity and EEM-PARAFAC extracted components with the exception of C3 ($R^2 = 0.469$) (Table 4 and Fig. 7d). It was because that with the sunshine duration hours increasing, the photo-degradation and microbial activities become stronger, leading to a more efficient transformation of labile fluorescence CDOM into non-fluorescence CDOM component (Song et al., 2013).

Table 4. Correlation coefficients (R) and significance levels (*p*) of the linear relationships between CDOM absorption, DOC, salinity and fluorescent components.

Figure 7. Relationships between CDOM absorption coefficient a(350) with a) F_{max}(C1), b) with F_{max}(C2), c) peak F_{max}(C1) versus F_{max}(C2), d) peak F_{max}(C3) versus DOC, e) Salinity versus DOC, f) Salinity versus F_{max}(C3).

4 Conclusions

In this study, the application of EEM-PARAFAC to characterize four fluorescent components under seasonal variation in CDOM was presented with 67 water samples

453 collected from June 2013 to April 2014 in the semi-arid region of the Songnen Plain.
454 Two humic-like and the protein-like components were identified using PARAFAC
455 model. The average fluorescence intensity of the four components differed under
456 seasonal variation from June 2013 to April 2014. The highest C1 1.02 nm^{-1} was
457 presented in February 2014 due to the condensed CDOM caused by ice formation in
458 winter. Especially in summer when quantities of rainfall take place and in winter
459 when water is frozen, the fluorescence intensity is dominated by tyrosine-like
460 component in rain and ice-melt water. Component 1 and 2 exhibited strong linear
461 correlation (R^2 = 0.633). There were significantly positive linear relationships
462 between F_{max} and CDOM absorption coefficient a(254) (R^2 = 0.72, 0.46, $p < 0.01$),
463 a(280) (R^2 = 0.77, 0.47, $p < 0.01$), a(350) (R^2 = 0.76, 0.78, $p < 0.01$) for two
464 humic-like components (C1 and C2), respectively. A weak relationship (R^2 = 0.42)
465 was found between DOC and component 3 from the decay of plants through
466 microbial activity or the pollution from human and animal wastes. Most importantly, a
467 significant relationship (R^2 = 0.931) was found between salinity and DOC. However,
468 almost no obvious correlation was found between salinity and EEM-PARAFAC
469 extracted components except C3 (R^2 = 0.469), though the correlation was not as
470 strong as with DOC concentration.

471

472 **Acknowledgements**

473 The research was jointly supported by the “One Hundred Talents” program from

Chinese Academy of Sciences and the National Natural Science Foundation of China (No. 41171293). The authors thank Zhi Ding, Ying Guan, Lei Liu and Ming Wang for their persistent assistance with both field sampling and laboratory analysis.

References

APHA/AWWA/WE F.: Standard Methods for the Examination of Water and Wastewater, Washington, DC: American Public Health Associstion, 1998.

Aiken, G. R., McKnight, D. M., Thorn, K. A., and Thurman, E. M.: Isolation of hydrophobic organic-acids from water using nonionic macro porous resins, Org. Geochem., 18, 567-573, 1992.

Andersen, C. M., and Bro, R.: Practical aspects of PARAFAC modeling of fluorescence excitation-emission data, J. Chemom., 17, 200-215, 2003.

Andersso, C. A., and Bro. R.: The N-way Toolbox for MATLAB, Chemom. Intell. Lab. Syst., 52, 1–4, 2000.

Babin, M., Stramski, D., Ferrari, G. M., Claustre, H., Bricaud, A., Obolensky, G., and Hoepffner, N.: Variations in the light absorption coefficients of phytoplankton, nonalgal particles, and dissolved organic matter in coastal waters around Europe, J. Geophys. Res., 108, 3211-3230, 2003.

Baker, J. D., Dubnick, A., Lyons, W. B., and Chin, Y. P.: Changes in Dissolved Organic Matter (DOM) Fluorescence in Proglacial Antarctic Streams, Arct. Antarct. Alp. Res., 45, 305-317, 2013.

Barker, J. D., Sharp, M. J., Fitzsimons, S. J., and Turner, R. J.: Abundance and dynamics of dissolved organic carbon in glacier systems, Arct. Antarct. Alp. Res., 38, 163–172, 2006.

Barker, J. D., Sharp, M. J., and Turner, R. J.: Using synchronous fluorescence spectroscopy and principal components analysis to monitor dissolved organic matter dynamics in a glacier system, Hydrol. Processes, 23, 1487–1500, 2009.

Barker, J. D., Klassen, J. L., Sharp, M. J., Fitzsimons, S. J., and Turner, R. J.: Detecting biogeochemical activity in basal ice using fluorescence spectroscopy, Ann. Glaciol., 51, 47–55, 2010.

Baker, A., Ward, D., Lieten, Shakti H., Periera, R., Simpson, Ellie C., and Slater, M.: Measurement of protein-like fluorescence in river and waste water using a handheld spectrophotometer, Water Res., 38, 2934-2938, 2004.

Borisover, M., Laor, Y., Parparov, A., Bukhanovsky, N., and Lado, M.: Spatial and seasonal patterns of fluorescent organic matter in Lake Kinneret (Sea of Galilee) and its catchment basin, Water Res., 43, 3104-3116, 2009.

Bricaud, A., Babin, M., Morel, A., and Claustre, H.: Variability in the chlorophyll-specific absorption coefficients of natural phytoplankton: Analysis and parameterization, J. Geophys. Res., 100, 13321–13332, 1995.

Bro, R.: PARAFAC tutorial and applications, Chemom. Intell. Lab. Syst., 38, 149-171, 1997.

Bro, R.: Exploratory study of sugar production using fluorescence spectroscopy and multi-way analysis, Chemom. Intell. Lab. Syst., 46,133-147, 1999.

517 Cheng, Y. Y., Guo, W. D., Long, A. M., and Chen, S. Y.: Study on optical
518 characteristic of chromophoric dissolved organic matter in rainwater by
519 fluorescence excitation-emission matrix and absorbance spectroscope (Article in
520 Chinese), Spectrosc. Spect. Anal., 30, 2413-2416, 2010.

521 Coble, P. G.: Characterization of marine and terrestrial DOM in seawater using
522 excitation-emission matrix spectroscopy, Mar. Chem., 51, 325–346, 1996.

523 Coble, P. G.: Marine optical biogeochemistry: the chemistry of ocean color, Chem.
524 Rev., 107, 402-418, 2007.

525 Coble, P. G., Del Castillo, C. E., and Avril, B.: Distribution and optical of CDOM in
526 the Arabian Sea during the 1995 Southwest Monsoon, Deep-Sea Res. part II, 45,
527 2195–2223, 1998.

528 Cory, R. M., and McKnight, D. M.: Fluorescence spectroscopy reveals ubiquitous
529 presence of oxidized and reduced quinines in dissolved organic matter, Environ.
530 Sci. Technol., 39, 8142-8149, 2005.

531 DelCastillo, C. E., Coble, P. G., Morell, J. M., Lopez, J. M., and Corredor, J. E.:
532 Analysis of the optical propertiesof the Orinoco River plume by absorption and
533 fluorescence spectroscopy, Mar. Chem., 66, 35–51, 1999.

534 Duarte, C. M., Montes, C., Cole, J. J., Striegl, R. G., Melackand, J., and Downing, J.
535 A.: CO_2 emissions from saline lakes: Aglobal estimate of asurprisingly large flux,
536 J. Geophys. Res. Biogeosci., 113, G04041, 2008.

537 Fellman, J. B., Hood, E., and Spencer, R. G. M.: Fluorescence spectroscopy opens

538 new windows into dissolved organic matter dynamics in freshwater ecosystems:
539 A review, Limnol. Oceanogr., 55, 2452-2462, 2010.

540 Guo, W. D., Xu, J., Wang, J. P., Wen, Y. G., Zhou, J. F., and Yan, Y. C.:
541 Characterization of dissolved organic matter in urban sewage using excitation
542 emission matrix fluorescence spectroscopy and parallel factor analysis, J.
543 Environ. Sci., 22, 1728-1734, 2010.

544 Henderson, R. K., Baker, A., Murphy, K. R., Hambly, A., Stuetz, R. M., and Khan, S.
545 J.: Fluoresence as a potential monitoring tool for recycled water system: A
546 review, Water Res., 43, 863-881, 2009.

547 Helms, J. R., Stubbins, A., Ritchie, J. D., Minor, E. C., Kieber, D. J., and Mopper, K.:
548 Absorption spectral slopes and slope ratios as indicators of molecular weight,
549 source, and photo bleaching of chromophoric dissolved organic matter, Limnol.
550 Oceanogr., 53, 955–969, 2008.

551 Hua, B., Dolan, F., Mcghee, C., Clevenger, ThomasE., and Deng, B. L.: Water-source
552 characterization and classification with fluorescence EEM spectroscopy:
553 PARAFAC analysis, Int. J. Environ. Anal. Chem., 87, 135-147, 2007.

554 Hudson, N., Baker, A., and Reynolds, D.: Fluorescence analysis of dissolved organic
555 matter in natural, waste and polluted waters – a review, River Res. Appl., 23,
556 631–649, 2007.

557 Jaffe´, R., Boyer, J. N., Lu, X., Maie, N., Yang, C., Scully, N. M., and Mock, S.:
558 Source characterization of dissolved organic matter in subtropical

559 mangrove-dominated estuary by fluorescence analysis, Mar. Chem., 84, 195–210,
560 2004.

561 Larsson, T., Wedborg, M., and Turner, D.: Correction of inner-filter effect in
562 fluorescence excitation-emission matrix spectrometry using Raman scatter, Anal.
563 Chim. Acta., 583, 357-363, 2007.

564 Lawaetz, A. J., and Stedmon, C. A.: Fluorescence Intensity Calibration Using the
565 Raman Scatter Peak of Water, Appl. Spectrosc., 63, 936-940, 2009.

566 Mayer, L. M., Schick, L. L., and Loder, T. C.: Dissolved protein fluorescence in two
567 Maine estuaries, Mar. Chem., 64, 171–179, 1999.

568 Mcknight, D. M., Boyer, E. W., Westerhoff, P. K., Doran, P. T., Kulbe, T., and
569 Andersen, D. T.: Spectrofluorometriccharacterization of dissolved organic
570 matter for indication of precursor organic material and aromaticity, Limnol.
571 Oceanogr., 46, 38–48, 2001.

572 Song, C. C., Wang, L. L., Guo, Y. D., Song, Y. Y., Yang, G. S., and Li, Y. C.: Impacts
573 of natural wetland degradation on dissolved carbon dynamics in the Sanjiang
574 Plain, Northeastern China, J. Hydrol., 398, 26-32, 2011.

575 Song, K. S., Zang, S. Y., Zhao, Y., Du, J., Lin, L., Zhang, N. N., Wang, X. D., Shao, T.
576 T., Guan, Y., and Liu, L.: Spatiotemporal characterization of dissolved carbon
577 for inland waters in semi-humid/semiarid region, China, Hydrol. Earth Syst.
578 Sci., 17, 4269-4281, 2013.

579 Spencer, R. G. M., Hernes, P. J., Ruf, R., Baker, A., Dyda, R. Y., Stubbins, A., and
580 Six, J.: Temporal controls on dissolved organic matter and lignin
581 biogeochemistry in apristine tropical river, J. Geophys. Res. Biogeosci., 115,
582 G03013, 2010.
583 Stedmon, C. A., and Bro, R.: Characterizing dissolved organic matter fluorescence
584 with parallel factor analysis: a tutorial, Limnol. Oceanogr. Methods, 6, 572-579,
585 2008.
586 Stedmon, C. A., and Markager, S.: Tracing the production and degradation of
587 autochthonous fractions of dissolved organic matter by fluorescence analysis,
588 Limnol. Oceanogr., 50, 1415-1426, 2005.
589 Stedmon, C. A., Markager, S., and Bro, R.: Tracing dissolved organic matter in
590 aquatic environments using a new approach to fluorescence spectroscopy, Mar.
591 Chem., 82, 239-254, 2003.
592 Stedmon, C. A., Thomas, D. N., Granskog, M., Kaartokallio, H., Papadimitriou, S.,
593 and Kuosa, H.: Characteristics of dissolved organic matter in Baltic coastal sea
594 ice: allochthonous or autochthonous origins? Environ. Sci. Technol., 41,
595 7273–7279, 2007.
596 Thomas K. B.: Under Landfast ice. Arctic, 36, 328-340, 1983.
597 Tranvik, L. J., Downing, J. A., Cotner, J. B., Loiselle, S. A., Striegl, R. G., Ballatore, T.
598 J., Dillon, P., Finlay, K., Fortino, K., Knoll, L. B., Kortelainen, P. L., Kutser, T.,
599 Larsen, S., Laurion, I., Leech, D. M., McCallister, S. L., McKnight, D. M.,

600 Melack, J. M., Overholt, E., Porter, J. A., Prairie, Y., Renwick, W. H., Roland, F.,
601 Sherman, B. S., Schindler, D. W., Sobek, S., Tremblay, A., Vanni, M. J.,
602 Verschoor, A. M., Wachenfeldt, E. V., and Weyhenmeyer, G. A.: Lakes and
603 reservoirs as regulators of carbon cycling and climate, Limnol. Oceanogr., 54,
604 2298–2314, 2009.

605 Uusikiv, J., Vahatal, A.V., Granskog, M.A., Sommaruga, R.: Contribution of
606 mycosporine-like amino acids and colored dissolved and particulate matter to
607 sea ice optical properties and ultraviolet attenuation. Limnol. Oceanogr., 55,
608 703–713, 2010.

609 Wharton, R. A., Jr., McKay, C. P., Clow, G. D., and Andersen, D. T.: Perennial ice
610 covers and their influence on Antarctic lake ecosystems. Antarct. Res. Ser., 59,
611 53–70, 1993.

612 Yamashita, Y.: Assessing the dynamics of dissolved organic matter (DOM) in coastal
613 environments by excitation emission matrix fluorescence and parallel factor
614 analysis (EEM-PARAFAC), Limnol. Oceanogr., 53, 1900-1908, 2008.

615 Yamashita, Y., Cory, R. M., Nishioka, J., Kuma, K., Tanoue, E., and Jaffe´, R.,:
616 Fluorescence characteristics of dissolved organic matter in the deep waters of the
617 Okhotsk Sea and the northwestern North Pacific Ocean, Deep Sea Res. Part II,
618 57, 1478–1485, 2010.

619 Zhang, Y. L., Liu, X. H., Osburn, C. L., Wang, M. Z., Qin, B. Q., and Zhou, Y. Q.:
620 Photo bleaching response of different Source of Chromophoric Dissolved

Organic Matter Exposed to Natural Solar Radiation Using Absorption and Excitation-Emission Matrix Spectra, Plos one, 8, e77515, 2013.

Zhang, Y. L., Yin, Y., Feng, L. Q., Zhu, G. W., Shi, Z. Q., Liu, X. H., and Zhang, Y. Z.: Characterizing chromophoric dissolved organic matter in Lake Tianmuhu and its catchment basin using excitation-emission matrix fluorescence and parallel factor analysis, Water Res., 45, 5110-5122, 2011.

Zhang, Y. L., Zhang, E. L., Yin, Y., VanDijk, M. A., Feng, L. Q., Shi, Z. Q., Liu, M. L., and Qin, B. Q.: Characteristics and sources of chromophoric dissolved organic matter in lakes of the Yungui Plateau, China, differing in trophic state and altitude, Limnol. Oceanogr., 55, 2645-2659, 2010.

Zhang, Y. L., VanDijk, M. A., Liu, M. L., Zhu, G. W., and Qin, B. Q.: The contribution of phytoplankton degradation to chromophoric dissolved organic matter (CDOM) in eutrophic shallow lakes: Field and experimental evidence. Water Res., 43, 4685–4697, 2009.

649 Table 1. Mean value of water quality parameters from June 2013 to April 2014. Turb
650 denotes water turbidity; N denotes sampling numbers.
651

Sampling season	pH	Salinity (PSU)	Turb (NTU)	N
Jun.2013	8.54	0.40	166.20±108.73	15
Aug.2013	8.63	0.37	63.13±31.21	13
Feb.2014	8.35	0.70	21.33±15.87	17
Apr.2014	8.67	0.43	22.24±16.42	22
All	8.55	0.48	62.18±79.07	67

652
653
654
655
656
657
658
659
660
661
662
663
664
665
666
667
668
669
670
671
672
673

Table 2. Positions of the fluorescence maximum peaks of the four components identified by PARAFAC modeling in the present study compared with those previously identified. Secondary excitation maxima is given in brackets.

Component No	Ex_{max}(nm)	Em_{max}(nm)	Description and source	Components (Coble) and (Zhang)	Components (Stedmon and Markager)
C1	230 (300)	425	Marine humic-like (phytoplankton degradation)	M	6
C2	255 (350)	460	Terrstrialhumic-like	A and C	1 and 4
C3	225 (290)	360	Autochthonous tryptophan-like	T	
C4	220 (275)	320	Autochthonous tyrosine-like	B	8

Fluoresence peaks were named as Components (Coble) and (Zhang) by Coble et al. (1996, 1998) and Zhang et al. (2010, 2011), while as Componets (Stedmon and Markager) by Stedmon and Markager (2005).

Table 3. Mean values of DOC concentration and CDOM absorption coefficients groups at different seasons. S_R: the slope ratio of $S_{275\text{-}295nm}$: $S_{350\text{-}400nm}$.

Sampling season	a(254) m^{-1}	a(280) m^{-1}	a(350) m^{-1}	S_R	DOC mg L^{-1}	N
Jun.2013	38.39±9.23	25.98±6.38	5.73±1.68	1.29±0.16	31.84±14.67	15
Aug.2013	29.71±4.73	19.36±2.91	5.82±0.81	0.96±0.22	32.83±14.78	13
Feb.2014	52.88±18.13	34.62±11.54	6.36±2.17	1.18±0.11	55.04±20.00	17
Apr.2014	34.43±11.38	22.45±7.36	4.17±1.49	1.32±0.13	30.86±10.91	22
All	39.08±14.73	25.73±9.58	5.40±1.84	1.21±0.20	37.60±18.05	67

Table 4. Correlation coefficients (R) and significance levels (*p*) of the linear relationships between CDOM absorption, DOC, salinity and fluorescent components.

	a(254)	a(280)	a(350)	DOC	Salinity	C1	C2	C3	C4
DOC	0.711**	0.646**	0.294*	1.000**					
Salinity	0.650**	0.579**	0.159	0.965**	1.000**				
C1	0.850**	0.875**	0.873**	0.496**	0.383**	1.000**			
C2	0.677**	0.686**	0.885**	0.414**	0.270*	0.796**	1.000**		
C3	0.452**	0.417**	0.134	0.648**	0.685**	0.267*	0.103	1.000**	
C4	-0.040	-0.016	0.078	-0.101	0.135	0.084	0.069	0.225	1.000**

**p< 0.01 level ; *p<0.05 level.

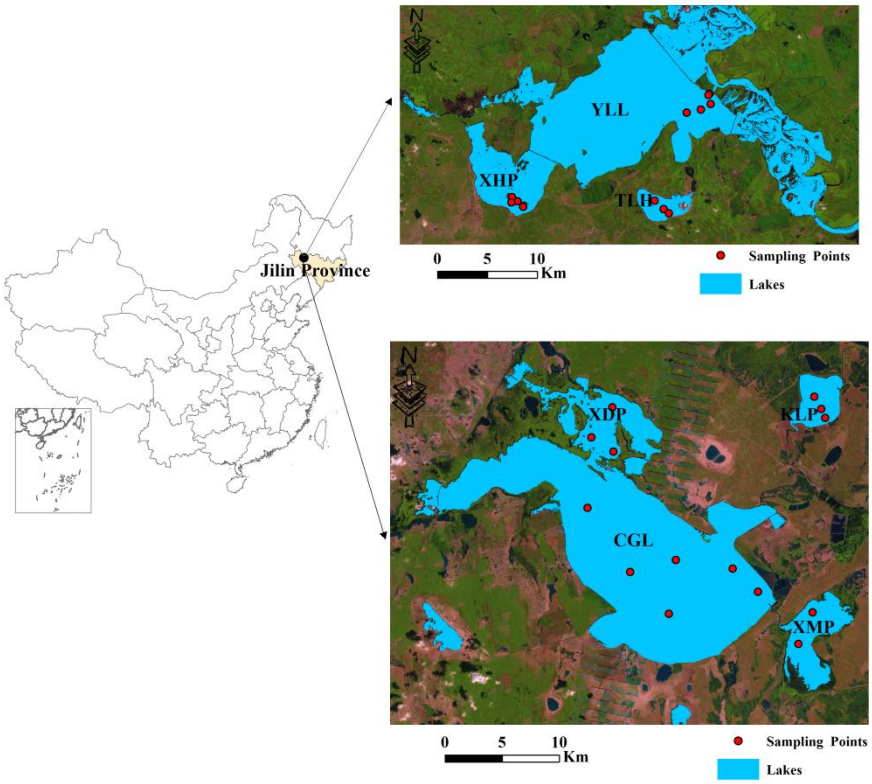

732
733
734

735 Figure 1. Locations of the water sampling sites for 7 lakes in the western part of Jilin

736 province, Northeast China.

737

738

739

740

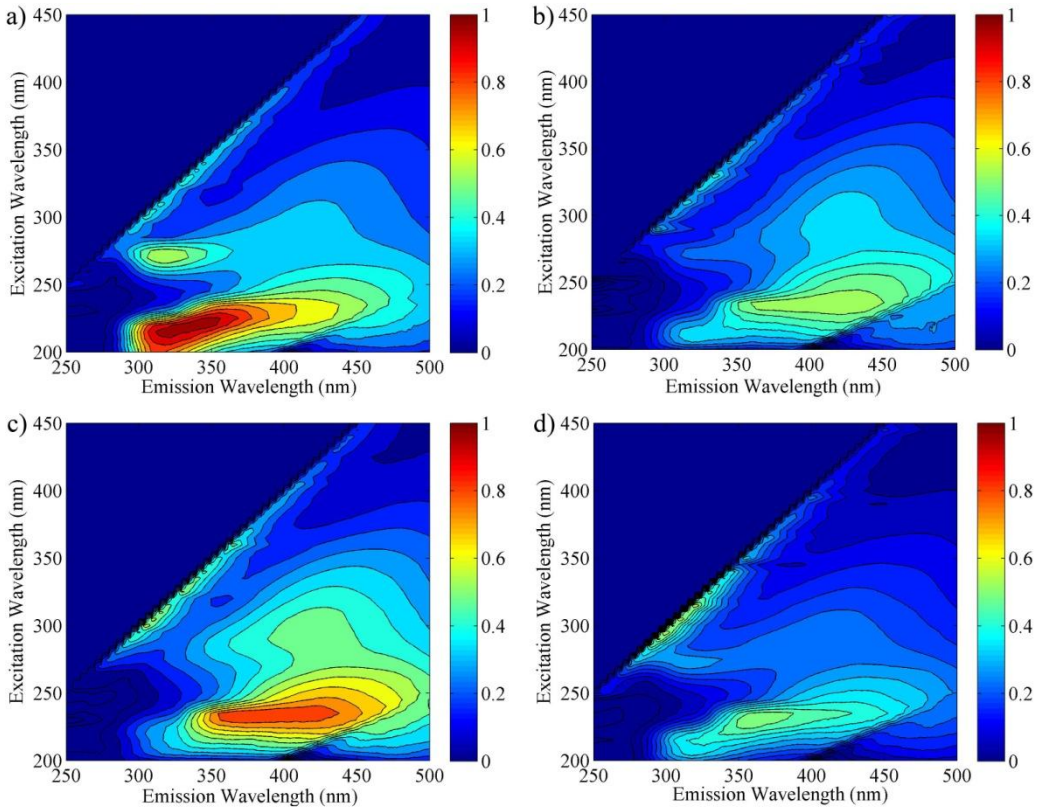

741

742

743 Figure 2. Examples of EEMs for one water sample from Xindianpao Lake in the

744 western part of Jilin province at different seasons a) June 2013; b) August 2013; c)

745 February 2014; d) April 2014 (Fluorescence is in Raman unit: nm^{-1}).

746

747

748

749

750

751

752

753

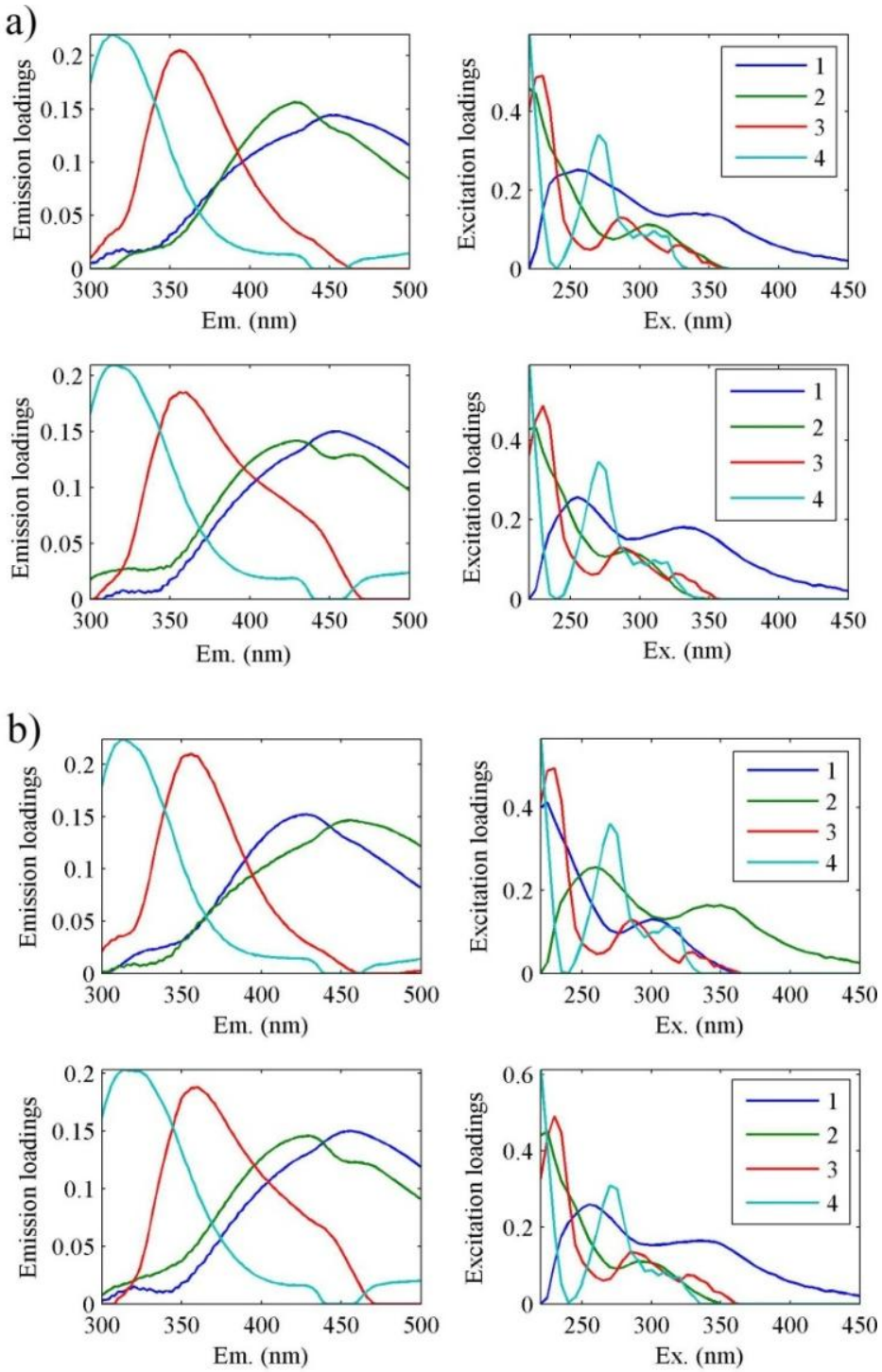

Figure 3. Results from split-half analysis (1-2 top a); 3-4 down b)) in PARAFAC models. The plots represent spectral shapes of the excitation and emission loadings from the two halves (1-2; 3-4 split -half analysis) modeling.

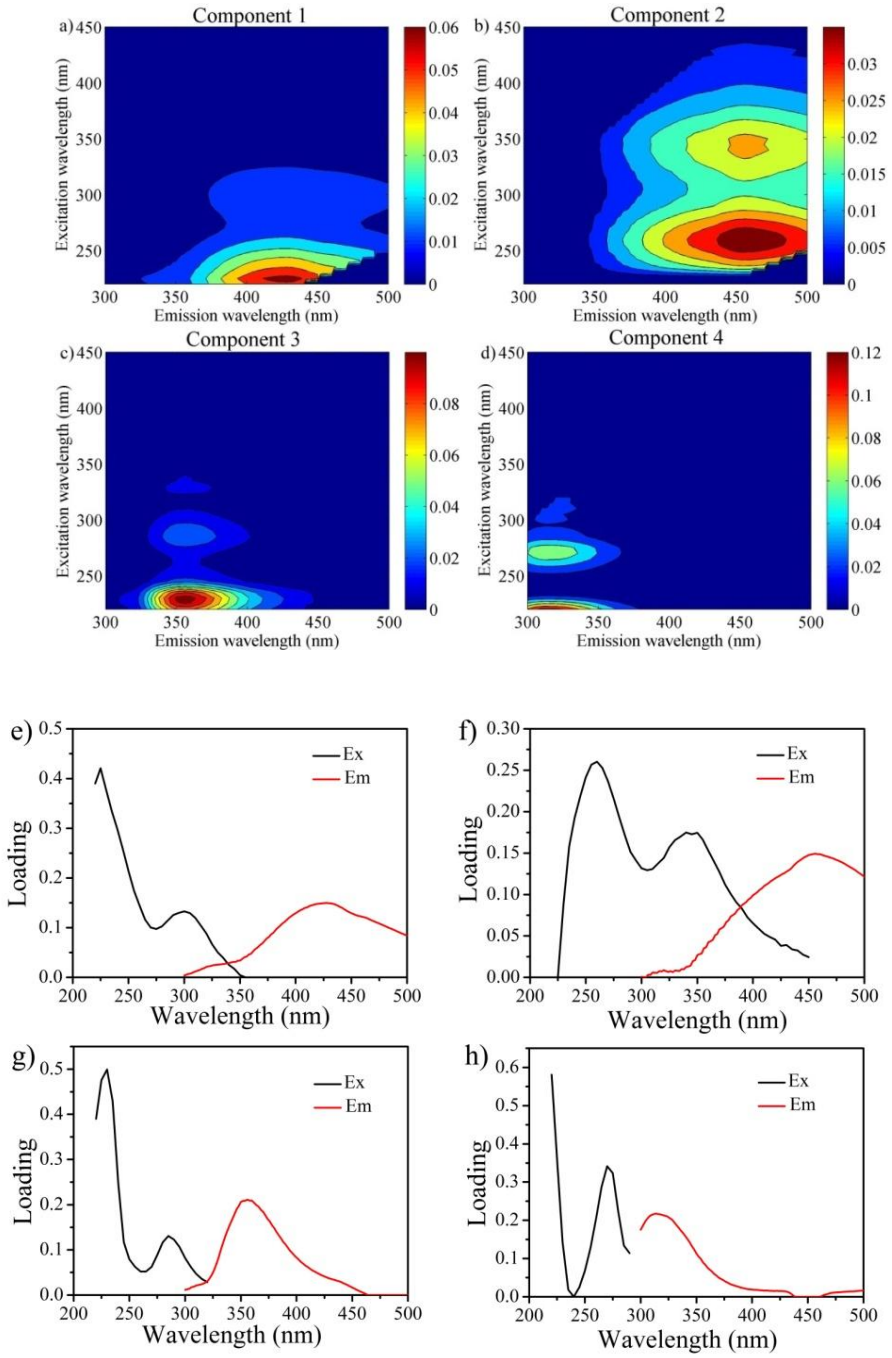

Figure 4. The PARAFAC model output shows the contour plots of the four PARAFAC fluorescent components (a-d) and excitation (black) and emission (red) loadings (e-h) of each component. Fluorescence is in Raman units: nm^{-1}.

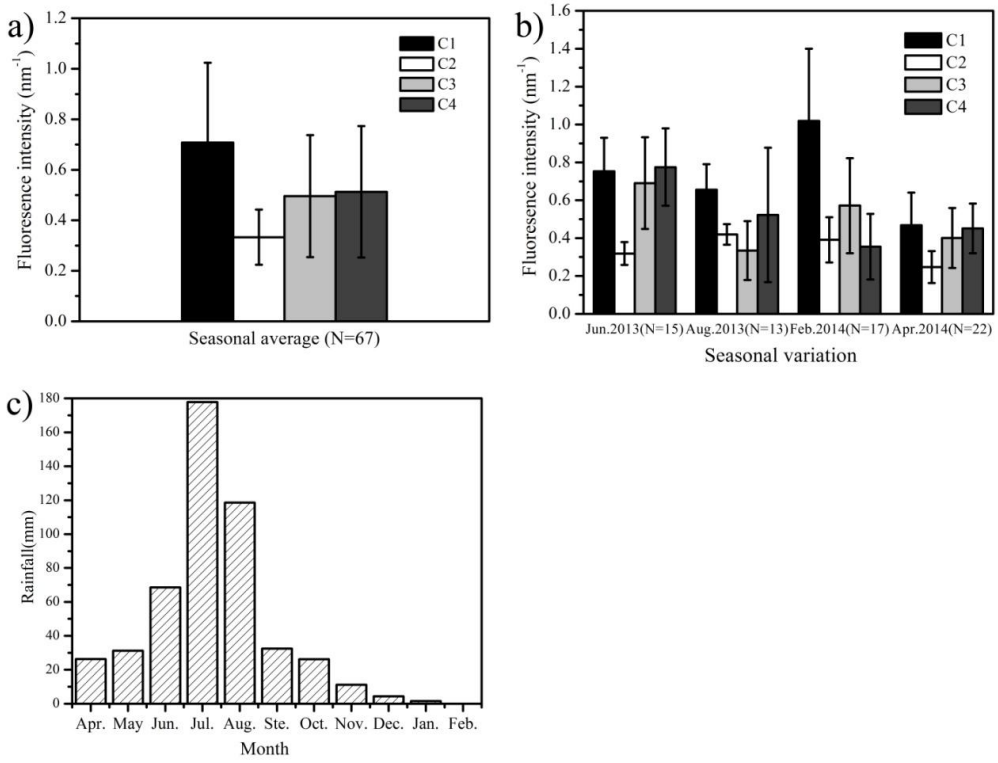

Figure 5. a) Seasonal average of F_{max} for EEM-PARAFAC components (C1, C2, C3 and C4) for lakes in the western part of Jilin province; b) Seasonal variation of the four EEM-PARAFAC components at different seasons; c) Monthly variation of rainfall for the lakes in western part of Jilin province from April 2013 to February 2014. The error bar represents standard deviations.

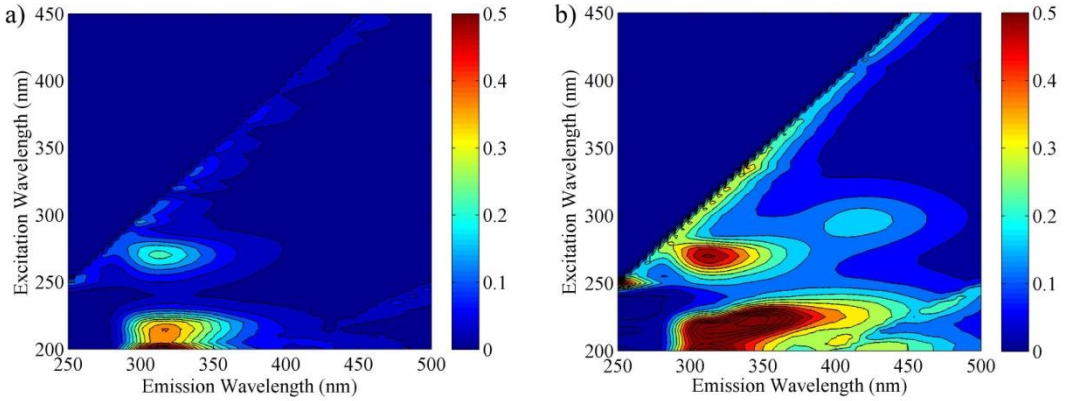

Figure 6. Representative examples of EEMs for a) lake ice-melt water sample, and b) rainwater CDOM in the western part of Jilin province (Raman: nm^{-1}).

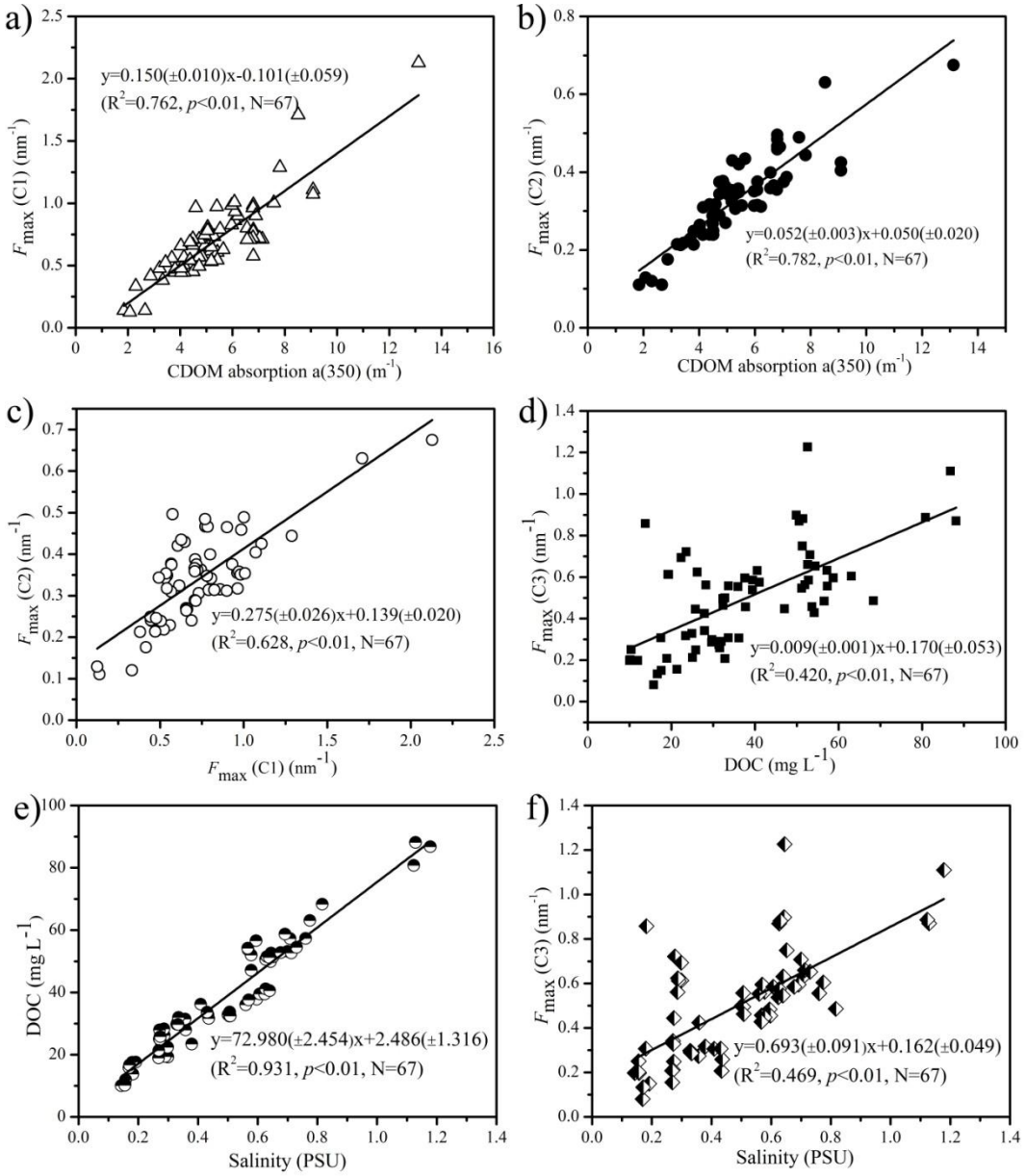

Figure 7. Relationships between CDOM absorption coefficient a(350) with a) F_{max}(C1), b) with F_{max}(C2), c) peak F_{max}(C1) versus F_{max}(C2), d) peak F_{max}(C3) versus DOC, e) Salinity versus DOC, f) Salinity versus F_{max}(C3).